Effect of Multiple Cation Electrolyte Mixtures on Rechargeable Zn–MnO2 Alkaline Battery

Benjamin J. Hertzberg,[†,#] An Huang,[‡,#] Andrew Hsieh,[†] Mylad Chamoun,[§] Greg Davies,[†] Joon Kyo Seo,[‡] Zhong Zhong,[♦] Mark Croft,[¶] Can Erdonmez,[⊥] Ying Shirley Meng,[∥] and Dan Steingart[*,†]

[†]Department of Mechanical and Aerospace Engineering, Princeton University, Princeton, New Jersey 08544, United States
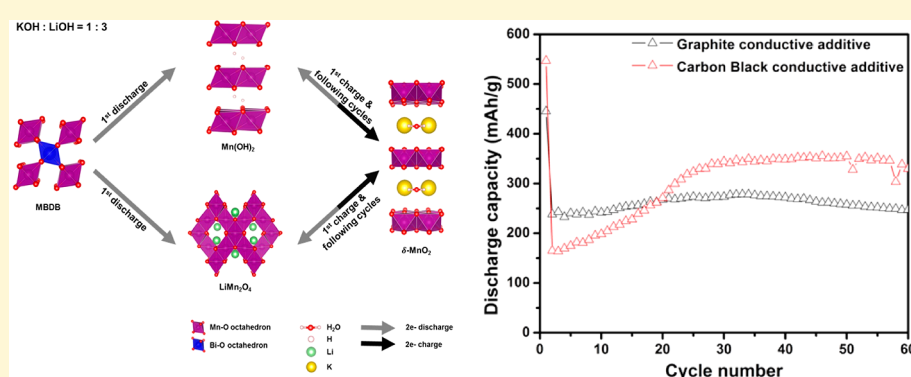
[‡]Department of Materials Science and Engineering, University of California San Diego, 9500 Gilman Drive, La Jolla, 92093, United States

[§]Department of Materials and Environmental Engineering, Stockholm University, Universitetsvagen 10, 114 18, Stockholm, Sweden

[∥]Department of NanoEngineering, University of California San Diego, 9500 Gilman Drive, La Jolla, 92093, United States

[⊥]Sustainable Technologies Division and [♦]Photon Sciences, Brookhaven National Laboratory, 2 Center Street, Upton, New York 11973, United States

[¶]Department of Physics and Astronomy, Rutgers University, 136 Frelinghuysen Road, Piscataway, New Jersey 08854-8019 United States

ABSTRACT: A Bi2O3 in β-MnO2 composite cathode material has been synthesized using a simple hydrothermal method and cycled in a mixed KOH–LiOH electrolyte with a range of concentrations. We show that, at a KOH:LiOH molar ratio of 1:3, both proton insertion and lithium insertion occur, allowing access to a higher fraction of the theoretical capacity of the MnO2 while preventing the formation of ZnMn2O4. This enables a capacity of 360 mAh/g for over 60 cycles, with cycling limited more by anode properties than traditional cathodic failure mechanisms. The structural changes occurring during cycling are characterized using electron microscopy and in situ synchrotron energy-dispersive X-ray diffraction (EDXRD) techniques. This mixed electrolyte shows exceptional cyclability and capacity and can be used as a drop-in replacement for current alkaline batteries, potentially drastically improving their cycle life and creating a wide range of new applications for this energy storage technology.

■ INTRODUCTION

Manganese–zinc primary alkaline batteries are a ubiquitous power source for a wide range of electronic devices today. These types of cells have high theoretical capacity and energy density, coupled with low cost, and are potentially suitable for a wide range of applications, including renewable energy storage and other grid applications, due to their high capacity, fast ionic conductivity, and low cost.[1] However, these types of cells have a wide range of different failure mechanisms, which taken as a whole prevent their effective use as secondary batteries.

Many of these failure mechanisms are associated with phase transformations in the electrolytic γ-MnO2 cathode. In Figure 1, we summarize the irreversible reaction of electrochemically prepared γ-MnO2 (EMD) in an alkaline battery, as previously reported in the literature.[2−6]

The most commonly accepted model of the phase transformation process proposes that the initial γ-MnO2 structure, which contains a 2 × 1 and 1 × 1 tunnel structures, is transformed into α-MnOOH and γ-MnOOH during the first electron reduction.[2−4] Proton intercalation can lead to the formation of either α-MnOOH, which maintains the 2 × 1 tunnel structure of γ-MnO2, or to the 1 × 1 tunnel structured γ-MnOOH, during which transformation the rearrangement of
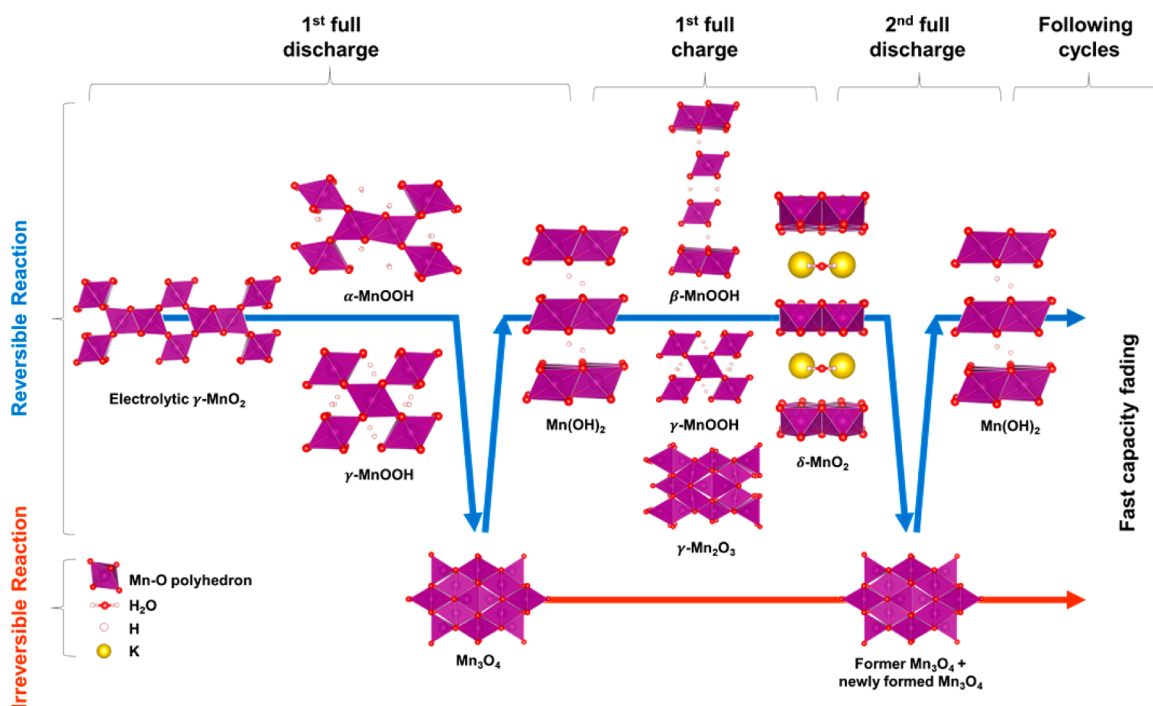
Figure 1. Reaction mechanism of γ-MnO$_2$ cathode in a standard alkaline battery.

Mn−O bonding occurs simultaneously with proton intercalation. In these phases, protons are complexed with the Mn atom, reducing the Mn oxidation state from 4+ to 3+. During the second electron reduction, Mn$_3$O$_4$[4,5] and Mn(OH)$_2$[5,6] are produced. If zinc is present in the electrolyte, ZnMn$_2$O$_4$ is produced instead.[7] ZnMn$_2$O$_4$ is not presented in Figure 1, as its formation from MnOOH, via the pathway 2MnOOH + Zn(OH)$_4^{2-}$ → ZnMn$_2$O$_4$ + 2H$_2$O + 2OH$^-$, is not an electrochemical process, and it is not considered to be an electrochemically active compound.[8,9,11]

Upon charging of the fully reduced phase, Mn(OH)$_2$ is converted to β-MnOOH, γ-MnOOH, and γ-Mn$_2$O$_3$, and subsequently to δ-MnO$_2$, also called birnessite.[6] δ-MnO$_2$ is a layered structure which may incorporate various cations, structural water, or both in the interlayer spacing, depending on the synthesis conditions.[10]

The irreversibility of MnO$_2$ is strongly correlated with the formation of the spinel phases Mn$_3$O$_4$ and ZnMn$_2$O$_4$, as shown in Figure 1. Once Mn$_3$O$_4$ is generated during the first discharge, this phase can only be partially reduced to Mn(OH)$_2$, and much of the produced spinel remains in the electrode even when it is fully discharged.[5] Meanwhile, ZnMn$_2$O$_4$ cannot be reduced to Mn(OH)$_2$ at all. During the first charge, only the oxidized Mn(OH)$_2$ is converted to MnOOH and δ-MnO$_2$, while the spinel phases have been found to be electrochemically inactive during oxidation.[6,12] After the first cycle, the cell will progressively lose capacity as more and more Mn$_3$O$_4$ is generated, leading to uneven potential distributions and the eventual failure of the cell. The addition of Zn to the electrolyte only accelerates this process, as ZnMn$_2$O$_4$ is even more electrochemically inert than Mn$_3$O$_4$. Local potential gradients can trigger this transformation at electrode-averaged depths of discharge as low as 20%, depending on the construction of the electrode.[11,13] This is a major failure mode of all rechargeable cells that use MnO$_2$ as a cathode material, especially those using Zn as a counter electrode.[7]

Varying individual factors of the EMD microstructure, such as the Mn stoichiometry, surface area, or cation vacancy fraction has little to no impact on the long-term cyclability of the cell, as crystallographic changes produced by charging and discharging the cell dominate the system, leading to the loss of the EMD crystal structure after the first full cycle.[14] Alternative methods for developing alkaline cells with superior cyclability include MnO$_2$−C composites[15,16] and doping MnO$_2$ with materials such as Bi, Ba, Ti, or Ni.[12,17−20] The modified materials have increased depth of discharge, and Bi and Ba doped materials in particular have high performance. However, doping has yet to solve the problem of Zn poisoning; when cycled in an electrolyte containing zinc ions, doped cathodes still form electrochemically inactive hetaerolite.[21] Another approach used for the prevention of hetaerolite formation is the use of alternative electrolytes. To resolve the issue of hetaerolite formation, LiOH has been used instead of KOH in MnO$_2$−Zn cells. When a saturated LiOH electrolyte is used instead of KOH, discharge capacity retention of at least 50% is extended from as little as 2 cycles to more than 40. This enhancement in cyclability may be attributable to the alternate insertion mechanism: rather than forming MnOOH and Mn(OH)$_2$ via proton insertion, reduction of MnO$_2$ in a LiOH electrolyte results in lithium insertion, forming the Li$_x$MnO$_2$ $(0 < x < 1)$ phase.[22] Without the formation of its precursor phase, MnOOH, the irreversible ZnMn$_2$O$_4$ phase is not formed. However, the cell capacity is substantially reduced, from ~325 to ~150 mAh/g. The reduced capacity of MnO$_2$ cycled in pure LiOH electrolyte is due to the limited insertion capacity for Li in the MnO$_2$ structure. At most, only 1 Li ion can be inserted into the structure, and due to the poor ionic conductivity of Li+ ions in MnO$_2$, full insertion is rarely achieved. As in primary cells, the addition of transition and alkali metal oxides, such as MgO, Bi$_2$O$_3$, or BaO, can substantially improve the capacity and cyclability of MnO$_2$− Zn aqueous Li-ion batteries, in part by reducing the crystallinity

of the Li_xMnO_2 spinel and improving its ionic conductivity. However, none of these additives fundamentally change the insertion mechanism of the system, preventing proton insertion from occurring and limiting the maximum theoretical capacity of the cathode.[23−25]

In this work, a Bi_2O_3 in β-MnO_2 composite cathode material has been synthesized using a simple hydrothermal method and cycled in a mixed KOH−LiOH electrolyte with a range of concentrations. We show that, at a KOH:LiOH molar ratio of 1:3, both proton insertion and lithium insertion occur, allowing access to a higher fraction of the theoretical capacity of the MnO_2 while preventing the formation of $ZnMn_2O_4$. This enables a capacity of 360 mAh/g for over 60 cycles, with cycling limited more by anode properties than traditional cathodic failure mechanisms. The structural changes occurring during cycling are characterized using electron microscopy and in situ synchrotron energy-dispersive X-ray diffraction (EDXRD) techniques. This mixed electrolyte shows exceptional cyclability and capacity and can be used as a drop-in replacement for current alkaline batteries, potentially drastically improving their cycle life and creating a wide range of new applications for this energy storage technology.

■ EXPERIMENTAL METHODS

MnO_2 Synthesis. Our active cathode material, a Bi_2O_3 in β-MnO_2 composite (MBDB), was prepared by a thermal decomposition process with a mixture consisting of $Mn(NO_3)_2 \cdot 4H_2O$ (Sigma-Aldrich, purum p.a., >97.0%), $Bi(NO_3)_3 \cdot 5H_2O$ (Sigma-Aldrich, ACS reagent grade, > 98.0%), and nitric acid (Sigma-Aldrich, ACS reagent grade, 70%)

Two different solutions were prepared: (1) 50 g of $Mn(NO_3)_2 \cdot 4H_2O$ in 80 mL of H_2O and (2) 4.27 g of $Bi(NO_3)_3 \cdot 5H_2O$ in 18.6 mL of H_2O and 6.4 mL of HNO_3. They were mixed separately first to ensure full dissolution of the precursors before being mixed together. The final solution was mixed using a magnetic stir-plate while heated by incrementally increasing the temperature with steps of 5 °C/min and an end temperature of 125 °C. The evolution of oxidation was visually observable through color changes of the solution. The end oxidation state (4+) resulted in a black solution, which was kept in vacuum at 125 °C overnight to ensure that all NO_x gases produced from the decomposition of nitric acid were eliminated. The sample was taken out after 12 h and baked at 325 °C for 5 h in a conventional oven. Finally, the dried and solid material was ground using mortar and pestle to break up the agglomerates of material. Our process for producing undoped β-MnO_2 (pyrolusite) was identical to our process for producing MBDB, but left out the bismuth nitrate pentahydrate from solution 2.

Electrochemical Techniques. After production of MBDB powder, the electrodes were mixed with conductive additives and Teflon emulsion (Sigma-Aldrich) and dried in a vacuum oven at 125 °C for 1 h. Two separate sets of additives were used: graphite (Timcal KS6) and carbon black (Timcal Super C). The electrodes made using graphite were 45% MBDB, 45% graphite, and 10% PTFE, while the electrodes made using carbon black were 60% MBDB, 30% CB, and 10% PTFE. After the electrodes were cast and dried, they were embedded onto a perforated Ni mesh and pressed using a pressure of 138 MPa to calendar the electrodes. The pressed electrodes were then assembled into planar cells, using acrylic plates held together with screws to maintain compression. The counter electrode was Zn metal plate. The separator used was 1 layer of polyvinyl chloride and 2 layers of nonwoven cellulose (FV-4304, Freudenberg LLC). The electrodes made using a mixture of MBDB and carbon black had an areal loading of 0.064 g/cm^2 and a total active mass per cell of 0.2 g. After assembly, the cells were immersed in a small sealed beaker of electrolyte containing 5 mL of electrolyte and cycled, either at a C/3 rate, a C/20 rate, or a C/4.2 rate, as described. Constant current rates were calculated with a MnO_2 capacity of 616 mAh/g. The voltage range

used was 1.8 > V > 0.4. At the end of constant current charging, a constant voltage of 1.8 V was applied until the current dropped to 10% of the maximum constant current value. The cells were cycled using a MTI BST8-3 battery analyzer.

Electrochemical impedance spectroscopy studies were carried out on these cells using an AC amplitude of 10 mV and a frequency range from 10 mHz to 10 kHz, using a Solartron 1260 frequency response analyzer. To obtain resistance and diffusion parameters, an equivalent circuit model was applied to EIS measurements, using a standard Randles circuit.[26] R_s represents the resistance of the cell, including electrolyte and ohmic impedance. R_{ct} represents the charge transfer resistance occurring at the surface of the electrode. The constant phase element (CPE) accounts for the double layer capacitance. Z_w represents the Warburg resistance from ionic diffusion in the MnO_2 bulk, which originates from the diffusivity of both protons and lithium ions in our case. The CPE is defined by two constraint parameters: CPE-T, the capacitance from an ideal double-layer capacitor, and CPE-P, a measurement of surface tortuosity.

SEM, XRD, and Surface Area Characterization. Scanning electron microscopy micrographs were produced using a Philips XL 30 environmental scanning electron microscope (ESEM), operated at an accelerating voltage of 20 kV. Ex-situ XRD measurements were performed via powder diffraction XRD (pXRD) techniques, acquired using a Bruker D8 advanced diffractometer with a Bragg−Brentano θ−2θ geometry and Cu Kα source (λ = 1.54). The samples were scanned from 10 to 80 degree at a scan rate of 0.0125° s^{-1}. We used Brunauer−Emmett−Teller (BET) techniques to analyze the material, using a Micromeritics Instrument Corporation ASAP 2020 nitrogen sorption system. Our results showed that MBDB possessed a specific surface area of 23.9 m^2/g.

EDXRD. A small beaker cell, printed using a Form 1 3D printer (Formlabs), was assembled. The printed photolithography resin was used because of its demonstrated base stability and X-ray transparency. The printed photolithography resin was confirmed to be of high X-ray transparency. The electrode was cycled under noncompression conditions in a 1 M KOH + 3 M LiOH electrolyte, against a Zn plate counter electrode. A C/4.2 rate was used, without an initial C/20 cycle. Cycling conditions were otherwise identical to those described previously. Constant current−constant voltage battery discharge was done using an MTI BST8-3 battery analyzer. EDXRD experiments were conducted at the National Synchrotron Light Source (NSLS) on the 7-pole superconducting wiggler beamline X17B1 at Brookhaven National Laboratory (BNL). During battery testing, an incident X-ray beam was fired at the battery being tested, and the diffracted beam was detected at a fixed angle 2θ = 3°. The collimation slits were set to control the sizes of the incident and scattered beams, whereby the intersection of the two beam cross-sectional areas defined a gauge volume (GV). The careful positioning of the GV allowed diffraction data to be collected from a spatially well-defined location. The collimation slits were set for values of di = 50 μm and ds = 100 μm. This produces a GV with a flat parallelepiped shape: 50 μm in the x1-direction, approximately 1.4 mm in the x2-direction, and 2 mm in the x3-direction.[27] The battery was moved using an X-Y-Z stage to scan the GV across the cathode, collecting EDXRD data at 366 μm intervals, covering the thickness of the cell cathode with 3 individual scans. Data were collected at each point for 1 min as the cell was cycling. The incident beam was white beam radiation with an energy range of <20−200 keV. Attenuation of the beam while traveling through the cell was minimal above 50 keV, where diffraction data were analyzed. The EDXRD detector was a standard cryogenically cooled high-resolution Canberra intrinsic Ge detector. The cryostat was configured for operation in an inclined angle operation. The Ge single crystal of the EDXRD detector was 1 cm thick, in order to enhance high absorption efficiency of high energy X-rays (about 90% at 100 keV). The detector was mounted on the arm of a Huber diffractometer, with a lead-shielded diffraction beam path to attenuate extraneous X-rays scattered in the white beam radiation hutch.[27,28] A digital signal processor and an 8192-channel multichannel analyzer were used with the detector. X-ray energy calibration was performed using LaB6 and CeO$_2$ standards.
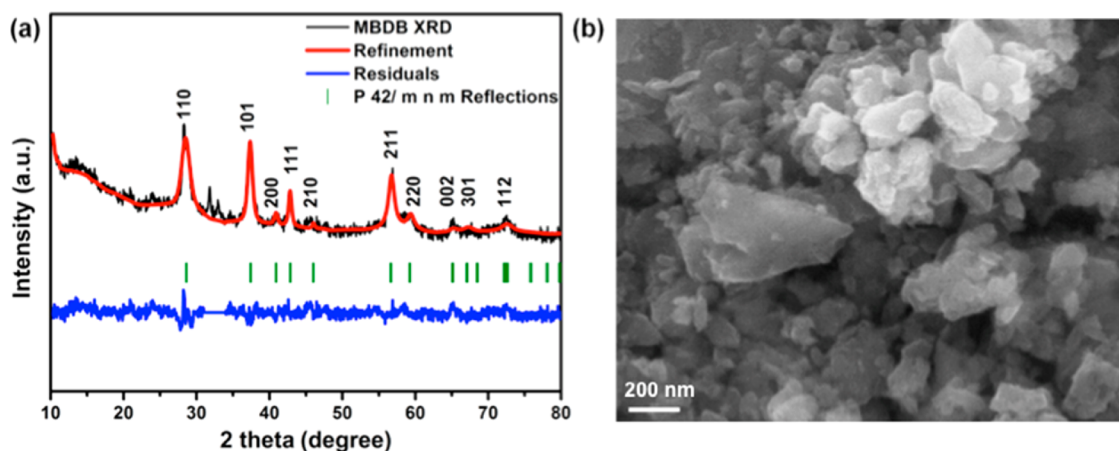
Figure 2. (a) Ex situ XRD spectra of MBDB, including as-scanned (black), the model produced by Rietveld Refinement (red), ICSD peak positions for pyrolusite (green), and the difference between as-scanned and model (blue), and (b) scanning electronic microscopy image (SEM).
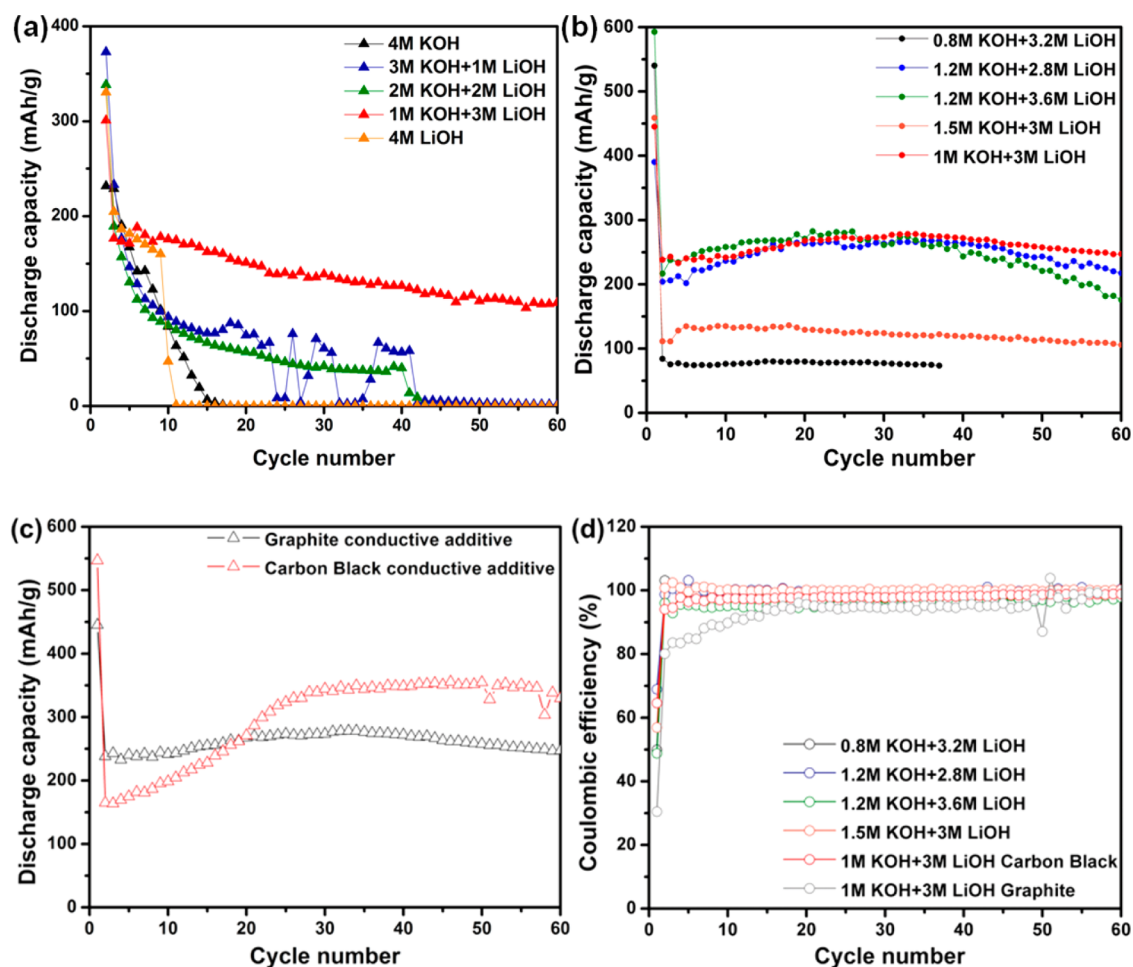

Figure 3. MBDB cells cycled at a (a) C/3 rate and (b) C/20 rate for the first cycle and C/4.2 rate for subsequent cycles against Zn plate in a range of different electrolytes. (c) MBDB cycled in 1 M KOH + 3 M LiOH at a C/20 rate for the first cycle and C/4.2 rate on subsequent cycles, demonstrating the effect of different conductive additives, carbon black and graphite, on capacity. (d) Coulombic efficiency of MBDB vs Zn cells in a range of electrolytes and different conductive materials.

RESULTS AND DISCUSSION

XRD spectra and scanning electron micrographs of the synthesized MBDB powder are shown in Figure 2a and b. A Rietveld refinement was conducted in order to elucidate the structure of the material and to better estimate the Bi:Mn stoichiometry. The refinement was performed using FullProf

software. From Figure 2a, the peaks at 31–34° are attributed to a Bi_2O_3 diffraction (ICSD 417638) while the rest of the peaks are well matched with β-MnO_2 (ICSD 73716). The Bi_2O_3 peaks region (31–34°) is excluded to get a more precise refinement fit. These results showed that bismuth atoms replaced 3.5% of the manganese atoms in the (0,0,0) position.
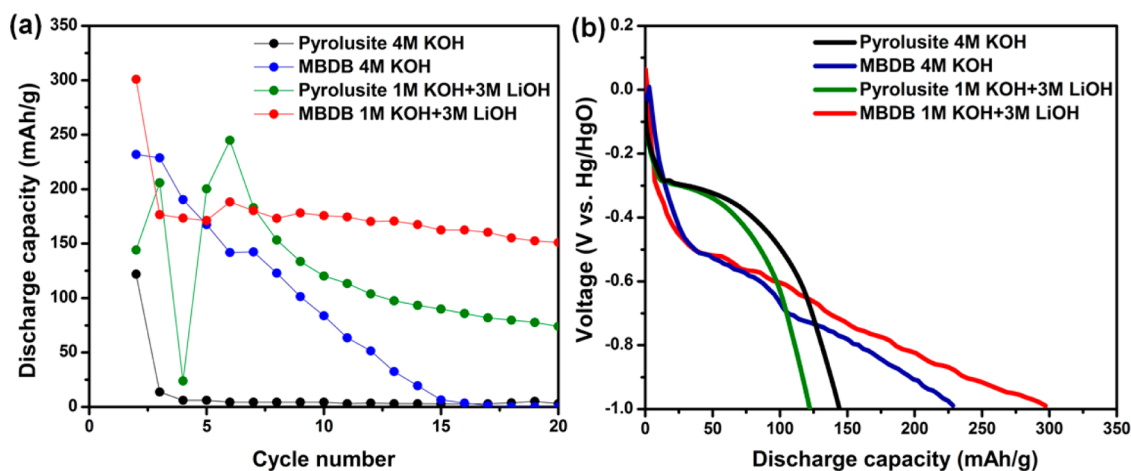
Figure 4. Comparison of the pyrolusite and MBDB cells with 4 M KOH or 1 M KOH+ 3 M LiOH cells, cycled at a C/3 rate in a three-electrode configuration against Hg/HgO reference electrode (+0.098 V vs SHE). (a) Specific discharge capacity vs cycle index; (b) discharge potential vs specific discharge capacity.

The oxygen atom is located at (0.3046, 0.3046, 0), and has occupancy of 2, with R_p and R_{wp} values of 9.8 and 15.4, respectively. The micrograph image (Figure 2b) indicates that the MBDB powder consists of agglomerated particles in a 50–100 nm diameter range. These results show that our synthesis method was able to produce a MBDB powder with a small particle size and with a Bi_2O_3 well distributed in a β-MnO_2. Although β-MnO_2 is often considered an electrochemically inactive phase, electrochemical activity is primarily governed by cation vacancies, which facilitate proton transport. It has previously been demonstrated that highly crystalline materials with few defects exhibit poor electrochemical activity regardless of their phase, and that proton transport can be facilitated either by the mixture of pyrolusite layers into the ramsdellite structure or by other defect types such as microtwinning. The MBDB produced via our method is highly defective, with accordingly increased electrochemical activity.[10]

Mixed electrolytes made up of a mixture of KOH and LiOH in a wide composition range, from 4 M KOH to 4 M LiOH, were tested at a C/3 rate. Subsequently, a second set of tests was performed in a more narrow composition range with slower rates, initially discharging and charging the cell at a C/20 rate for the first cycle, and subsequently charging it at a C/4.2 rate. These results are shown in Figure 3a and 3b, respectively.

When cycled at a C/3 rate, the 4 M KOH, 3 M KOH + 1 M LiOH, and 2 M KOH + 2 M LiOH cells show a similar pattern of behavior, with a rapid and exponential decline in capacity from an initial value of ~350 to ~75 mAh/g. The 1 M KOH + 3 M LiOH and 4 M LiOH cells, however, show a much smaller drop in capacity with cycling. The 4 M LiOH cell fails relatively rapidly due to passivation of the Zn plate, however, as the ZnO passivating film cannot dissolve well in a weak base such as LiOH.[29] The 1 M KOH + 3 M LiOH cell shows a capacity over 100 mAh/g for more than 50 cycles with relatively little fading after the first cycle. Subsequent tests at slower rates in a narrower composition range, shown in Figure 3b, demonstrate that the superior performance seen in the 1 M KOH + 3 M LiOH electrolyte cell is localized to a composition range of approximately 1:3 to 3:7 KOH:LiOH. Within this composition range, we see relatively high capacity, with a peak value of ~280 mAh/g. If the KOH:LiOH ratio is reduced to 1:4 or increased to 1:2, a dramatic loss of capacity occurs, reducing performance to ~125−75 mAh/g after the first cycle. This is presumably due to either the loss of the proton insertion mechanism for charge storage (when the KOH:LiOH ratio is reduced) or the development of electrochemically inactive hetaerolite (when the KOH:LiOH ratio is increased).

To further improve performance, we replaced the graphite conductive additive used in our electrodes with carbon black, a higher surface area conductive additive. These results are shown in Figure 3c. Carbon black is noted to improve overall performance in MnO_2 cathodes undergoing deep discharge by reducing the size of the product phase particles and enhancing overall electrode conductivity, at the cost of open circuit potential.[30,31] As predicted, cells assembled with carbon black instead of graphite exhibited ~200 mV lower open circuit potential, due to the interaction of the surface groups on the carbon black with the MnO_2. However, the higher surface area of the amorphous carbon significantly enhances interdigitation of the conductive additives and active material, leading to a substantial improvement of the overall capacity of the full cell, increasing capacity from ~280 to ~360 mAh/g. This is accomplished without reducing the average potential of discharge; instead, a larger fraction of the electrode capacity is accessible. The capacity of these cells is high enough that performance cannot be explained only by lithium insertion into the MnO_2. The maximum capacity of lithiated MnO_2, for a full first electron reduction to $LiMnO_2$, is 285 mAh/g. After ~60 cycles, the cell fails due to the complete dissolution of the Zn anode.

The impact of the electrolyte and conductive additives on Coulombic efficiency was also examined, as shown in Figure 3d. After the first cycle, the efficiency of every cell is over 80%. The high Coulombic efficiency after the initial capacity fade indicates that critical capacity fade mechanisms are stabilized in all cases, but that the electrolyte mix determines the extent of critical fade. Cells with higher capacity, such as those made with carbon black conductive additives, tend to exhibit lower efficiency, although once cell break-in is completed, the efficiency increases to ~95%. Cells made with graphite conductive additives exhibit Coulombic efficiency of ~99%. The reduced Coulombic efficiency of the cells made with carbon black conductive additives may be due to the poor oxidative stability of amorphous carbon as compared to that of graphite.
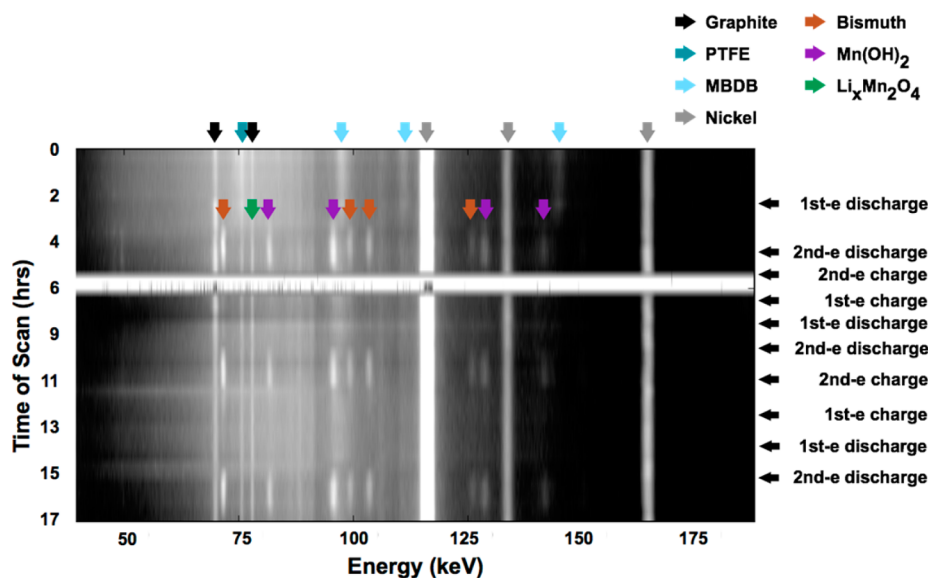
Figure 5. In situ EDXRD studies on a MBDB cell with graphite conductive additives cycled against zinc metal in 1 M KOH + 3 M LiOH. The colored vertical arrows indicate peaks associated with particular phases; the black horizontal arrows at right indicate the end of a specific charge or discharge stage of the MBDB electrode.
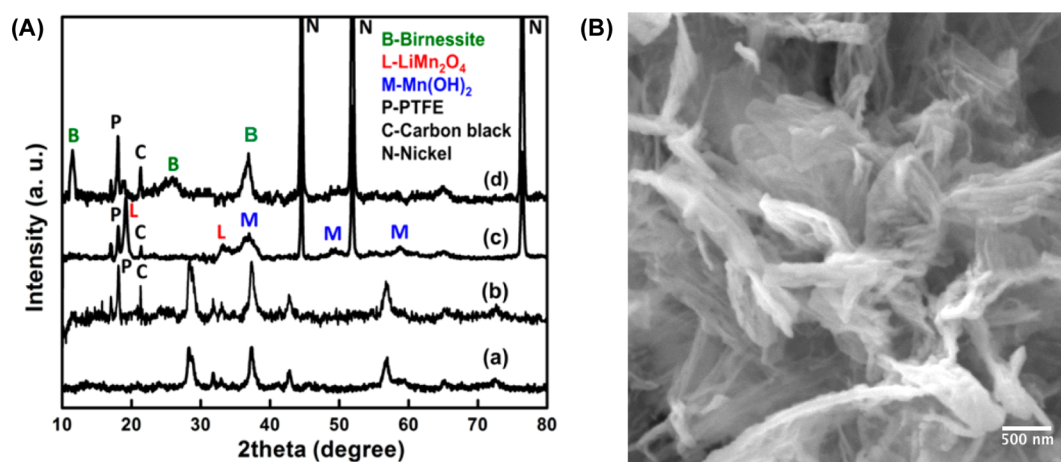

Figure 6. (A) Ex situ XRD patterns of structural evolution of the MBDB composite electrodes with carbon black conductive additives in 1 M KOH + 3 M LiOH at various states of discharge: (a) MBDB pristine powder, (b) MBDB pristine electrode, (c) after full discharge of the 1st cycle, and (d) after full recharge of 1st cycle. (B) High-resolution scanning electron microscopy (SEM) micrographs showing the microstructural change for MBDB electrodes cycled in 1 M KOH + 3 M LiOH after full recharge.

To better understand the impact of both the bismuth dopants and the mixed electrolyte on the phase transformation occurring in the cathode, we performed a careful galvanostatic analysis of the first discharge of MnO_2 cycled with Bi_2O_3 composite (MBDB) and without (pyrolusite) and in both pure KOH and 1 M KOH + 3 M LiOH electrolytes. These results are shown in Figure 4. Our results show that the second electron discharge regions of the bismuth-doped cells are much larger than those of the undoped cells, and tend to occur at a lower reduction potential. This is likely due to the fact that bismuth acts as a redox catalyst, stabilizing the structure and extending the discharge regime.[32] In addition, the presence of bismuth in the structure may promote the formation of Bi−Mn complexes, which inhibit the formation of undesirable products, such as Mn_3O_4; this may in turn enhance the overall capacity and retention of the cell.[20] Mn^{3+} is known to dissolve into electrolyte and be reduced to Mn^{2+}. These two dissolved species tend to react with each other, however, and produce

Mn_3O_4. The presence of bismuth in the structure enables it to dissolve into electrolyte and become the positively charged complex $Bi_6(OH)_{12}^{6+}$. This compound is known to combine with $Mn(OH)_2^{3-}$ or $Mn(OH)_2^{4-}$, forming Bi−Mn complexes, and thereby inhibiting the formation of the lower-cyclability Mn_3O_4 phase.[33−36] This may explain why a flatter and longer voltage profile regime is present in bi-doped samples, and why they generate higher capacity.[32] Figure 4b also shows that cells cycled in the 1 M KOH + 3 M LiOH electrolyte exhibit a less distinct separation between the first- and second-electron discharge plateaus, presumably due to the simultaneous insertion of lithium into the structure providing a secondary reduction mechanism.

These results indicate that the use of a mixed electrolyte with precisely balanced KOH:LiOH ratio can dramatically enhance the overall cyclability of a MnO_2−Zn cell. To elucidate the effects of this mixed electrolyte on the microstructural changes occurring within the MBDB cathode, EDXRD was performed
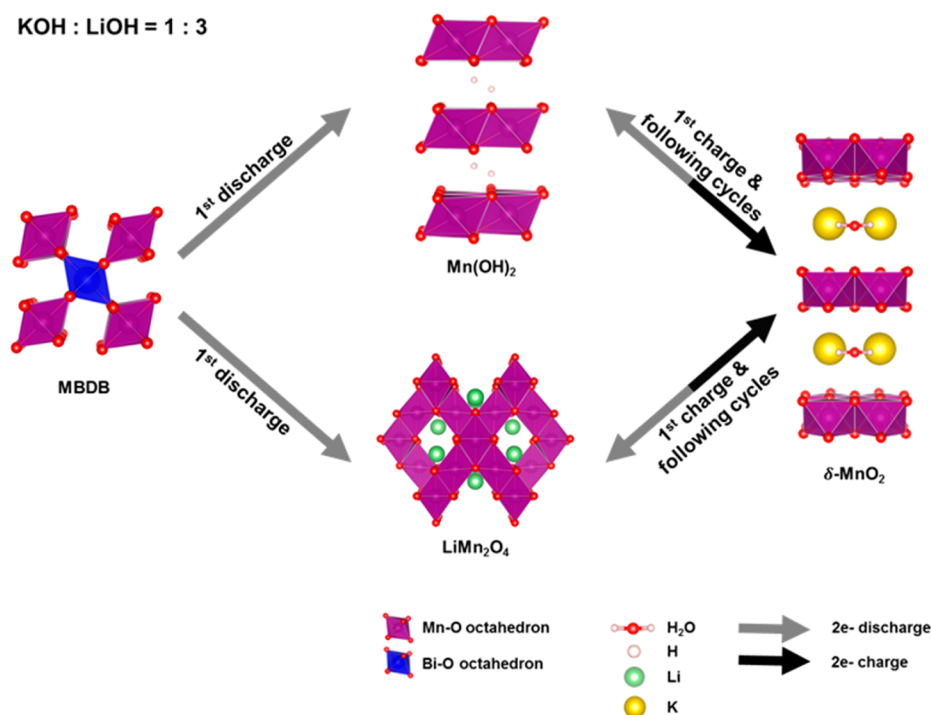
Figure 7. Proposed phase transformation of MBDB cell under KOH:LiOH = 1:3 electrolytes.

on a small-scale cell. This in situ study was performed at the X17B beamline at the National Synchrotron Light Source at Brookhaven National Laboratory, the results of which are shown below in Figure 5.

Our in situ studies showed that the MBDB is fully reduced to $Mn(OH)_2$, with peaks apparent at 81.42, 95.2, 128.5, and 141.4 keV. This confirms that proton insertion occurs in the electrode despite the presence of lithium ions. However, the increase in intensity during discharge of the peak at 77.8 keV suggests that $LiMn_2O_4$ is also present. The presence of both product phases simultaneously suggests that lithium and proton insertion occur simultaneously during reduction of the cathode. During reoxidation of the cathode, the MBDB structure that the electrode originally possessed is not recovered. In fact, within the range of photon energies scanned, no crystalline manganese oxide phases are present when the electrode is charged.

Conventional, ex situ XRD techniques were also carried out to characterize the cells with carbon black conductive additives at fully discharged (−1 V vs Hg/HgO) and fully recharged (+0.3 V vs Hg/HgO) states. The results are shown in Figure 6A.

As shown in the EDXRD results, when the electrode is fully discharged, a strong peak appears at 19°, equivalent to the peak at 77.8 keV in Figure 5, indicated the presence of $LiMn_2O_4$. The presence of $Mn(OH)_2$ is similarly indicated. For the fully recharged sample, however, a significant peak appears at 12°. The peak at this angle can be assigned to the birnessite family.[37] The resulting dramatic physical transformation, shown in Figure 6B, confirms an extensive change in the microstructure of the material after cycling. The absence of birnessite in Figure 5 is a product of the limited energy range of the EDXRD scan. On the basis of this information, we have included in Figure 7 a schematic of our best estimate of the structural transformations occurring in the MBDB material when cycled in 1 M KOH + 3 M LiOH.

As shown in Figure 7, the cathode is, in the first cycle, converted into a mixture of $LiMn_2O_4$ and $Mn(OH)_2$ at the fully discharged state when the 1 M KOH + 3 M LiOH electrolyte is used. This is followed by a transformation to the layered birnessite structure at the fully recharged state. The (111), (113), and (222) $LiMn_2O_4$ peaks, at 19.1, 33.9, and 44.9° respectively, continue to be visible in the fully recharged state, albeit at diminished relative intensity. This suggests that Li extraction from the cathode is not fully completed, presumably due to slow diffusion of Li through the spinel structure. This reaction is frequently considered rate-limiting in aqueous Li-ion cells. However, the partial extraction of lithium from the spinel phase will minimize the development of Jahn−Teller distortion, which may be caused by the presence of the spinel phase.[38] The absence of intermediate Mn^{3+} oxides, such as MnOOH or Mn_2O_3 (see Figure 1), may be explained by the simultaneous first- and second-electron reduction of the cathode.[11,39] We hypothesize that the exclusion of the intermediate Mn^{3+} phases formed during normal proton insertion in favor of lithiated Mn spinel phases is key to the role of the 1 M KOH + 3 M LiOH electrolyte in improving cyclability. The irreversible $ZnMn_2O_4$ phase is produced by reaction of these intermediates with solvated zincate ions.[11] The concentration of KOH is still high enough for a full second electron reduction of the MnO_2 to occur, resulting in the formation of $Mn(OH)_2$, but the protonated intermediates do not form. By contrast, when cycled in pure KOH, the irreversible phases $ZnMn_2O_4$ and Mn_3O_4 form in addition to $Mn(OH)_2$. While $Mn(OH)_2$ can be oxidized to birnessite, these irreversible phases cannot. Consequently, the fraction of irreversible products increases with each subsequent cycle. These results are further supported by the SEM images shown in Figure 8, in which the MBDB cathode is shown before cycling, in the fully discharged state (−1 V vs Hg/HgO), and in the fully recharged state (+0.3 V vs Hg/HgO).
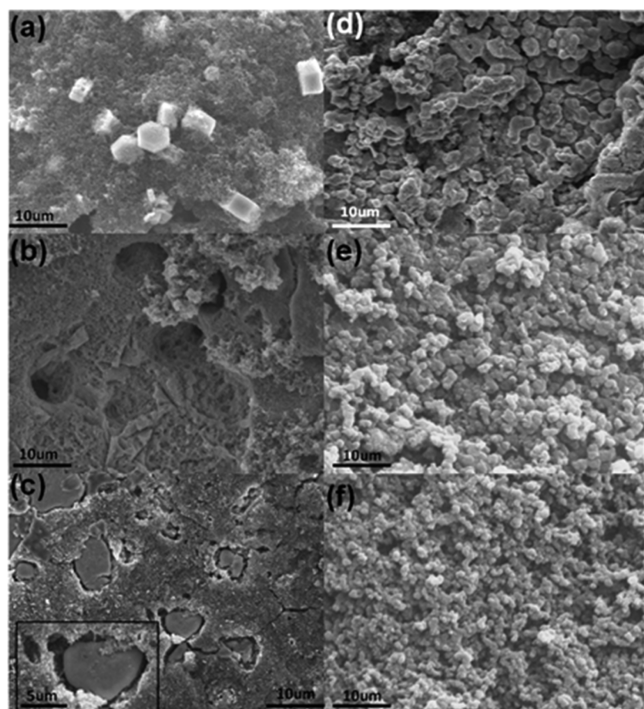
Figure 8. Scanning electron microscopy (SEM) micrographs demonstrating the change of morphology for MBDB electrodes with 4 M KOH electrolyte (a) after first cycle discharge, (b) after first cycle recharge, (c) after tenth cycle fully discharged, and with 1 M KOH + 3 M LiOH electrolyte (d) after first cycle discharge, (e) after first cycle recharge, (f) after tenth cycle fully discharged.

For the cell with 1 M KOH + 3 M LiOH, in the fully discharged state, the electrode is highly homogeneous, with 1-μm rounded particles of manganese-hydroxide-coated carbon black. During discharge, manganese dissolves and reprecipitates onto the conductive additives in the electrode as part of the Mn^{3+}/Mn^{2+} reduction, with the size of the product particles being limited by the electrical conductivity of the product phase. A similar effect occurs during the oxidation of the cathode active material.[36] When the electrode is recharged, the electrode appears to be mostly composed of rounded, small particles with a diameter of around 50 nm, which appear to be highly agglomerated. After 10 cycles in the fully discharged state, the particle size is reduced to 20-nm diameter, with a more discrete morphology. However, when the cell is cycled with only KOH as an electrolyte, the electrode is no longer homogeneous in the discharged state. Instead, large hexagonal particles with a 5-μm diameter are produced, coupled with much smaller, ~ 50 nm rounded particles. This is a radical change from the initial structure of the MBDB particles, as seen in Figure 2b. After subsequent oxidation of the electrode, larger agglomerated particles begin to form, creating void spaces in the previous contiguous electrode. By the tenth cycle, these agglomerated particles of electrochemically inactive material, presumably $ZnMn_2O_4$, take up a significant fraction of the electrode volume. The combination of the formation of inactive phases and physical disruption of the electrode may both contribute to the capacity fading of the cell. The microstructural and morphological changes of the MBDB cell cycled in 1 M KOH + 3 M LiOH is much more homogeneous than the pure KOH cell, which may be a factor in the superior capacity retention of the mixed electrolyte. The more

homogeneous morphological changes result in the decrease of formation of cracks and holes formation in the electrode, which may also enhance cycle life for the cell. The electrodes shown in Figure 8 were also studied via energy-dispersive X-ray spectroscopy (EDX). The electrode cycled in 4 M KOH showed a significant quantity of Zn, with a Zn:Mn atomic ratio of 1:8.11. This suggests that as much as ~24.7% of the MnO_2 in the electrode has been converted into $ZnMn_2O_4$. However, the cell cycled in 1 M KOH + 3 M LiOH showed no Zn present, suggesting that the formation of $ZnMn_2O_4$ had been completely averted.

We have also characterized the electrochemical impedance parameters of the MnO_2−Zn cell in order to understand its electrical properties. Electrochemical impedance spectroscopy (EIS) measurements were performed with three-electrode cell configurations, the results of which are shown in Figure 9.[26] The results were fitted to a standard Randles circuit to derive the electrochemical impedance characteristics of this system, which are shown in Table 1.
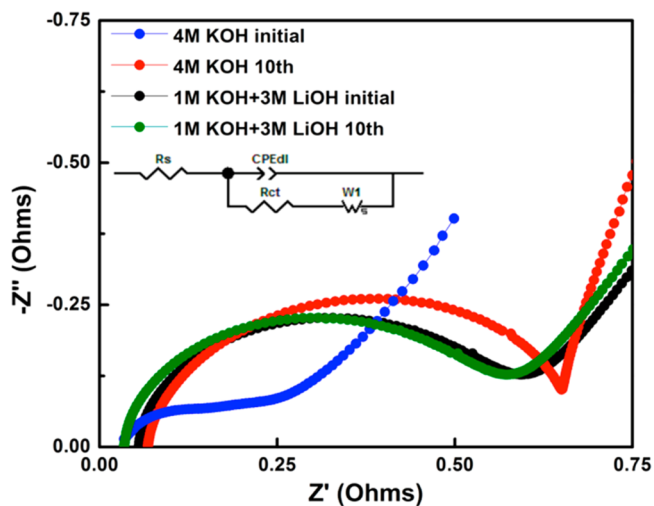

Figure 9. Electrochemistry impedance spectroscopy (EIS) analysis of a MBDB vs Zn cell in both KOH and 1 M KOH + 3 M LiOH conditions before the first cycle and after the tenth cycle.

The fitting parameters for our EIS results are shown in Table 1. When MnO_2 is cycled in 1 M KOH + 3 M LiOH instead of 4 M KOH, the Ohmic impedance (R_s), double-layer capacitance (C_{dl}), and charge transfer impedance (R_{ct}) are all significantly increased. This suggests that a different reduction reaction, presumably Li insertion, is rate-limiting in cells using a mixed electrolyte rather than pure KOH. As a result, the Mn^{4+}/Mn^{3+} redox couple is dominated by the process of Li insertion, rather than proton insertion, as is the case in EMD (see Figure 1). Changes in R_s and R_{ct} after cycling also are significantly impacted by our choice of electrolyte. R_s and R_{ct} for the MBDB cell in 1 M KOH + 3 M LiOH electrolyte are slightly smaller at the tenth cycle than in their initial state, suggesting that the surface properties of the electrode do not change significantly with cycling, and the overall shape of the Nyquist plot is quite similar for both points in the cell lifetime. The cell cycled with 4 M KOH showed lower R_{ct} in the pristine state than the cell with 1 M KOH+3 M LiOH, but by the tenth cycle, the R_{ct} is substantially higher than that of the cell in its pristine state. This result may be correlated to the microstructural changes

Table 1. Fitting Parameters of the EIS Analysis Obtained from the Equivalent Circuit Model

sample ID	state	R_s (Ω)	R_{ct} (Ω)	W_1 (Ω s$^{-1/2}$)	CPE_{dl} (F s^{a-1})
MBDB - 4M KOH	as prepared	0.029	0.183	0.287	0.0330 (a = 0.684)
MBDB - 4M KOH	10th cycle	0.068	0.583	0.580	0.0019 (a = 0.877)
MBDB - 1 M KOH + 3 M LiOH	as prepared	0.054	0.544	0.646	0.0021 (a = 0.871)
MBDB - 1 M KOH + 3 M LiOH	10th cycle	0.034	0.538	0.688	0.0016 (a = 0.897)

previously described, as much of the cell has been converted into an electrochemically irreversible and inert phase.

CONCLUSIONS

A study on the impact of mixed mixtures of KOH and LiOH electrolytes in MnO_2–Zn cells has been undertaken. It was found that, depending on the exact composition of the electrolytes, either proton insertion, lithium insertion, or a combination of both mechanisms can dominate the reduction of the MnO_2. When lithium insertion or combined lithium–proton insertion is the dominant reduction mechanism, zinc poisoning reactions do not occur, allowing much greater cycle lifetimes for the cell: up to 60 cycles with minimal loss of capacity, limited primarily by the dissolution or passivation of our Zn plate anode. At the correct electrolyte composition, consisting of 1 M KOH and 3 M LiOH, both lithium and proton insertion mechanisms occur, enabling full two-electron reduction of the MnO_2. We have analyzed the structural and microstructural changes occurring in the electrode using a variety of techniques, including in situ EDXRD, conventional ex-situ XRD, and scanning electron microscopy techniques. We have concluded that this improvement in cyclability is due to the exclusion of intermediate protonated Mn^{3+} phases produced during normal proton insertion in favor of lithiated Mn spinel phases that are not susceptible to Zn poisoning. We have also analyzed the role of bismuth in the cathode material, concluding that bismuth acts as a redox catalyst, stabilizing the structure and extending the second-electron discharge regime. With appropriate cycling protocols and additives, the capacity of the MnO_2 cathode is increased dramatically, up to as much as 360 mAh/g. Because of the high capacity of the MnO_2–Zn cell, the theoretical energy density of a rechargeable alkaline cell could be as high as 100−150 Wh/kg, with extremely low material costs and exceptional safety compared to other rechargeable battery technologies (probably less than 60$ per kilowatt hour). Rechargeable alkaline batteries using mixed electrolytes show significant potential for a sustainable energy storage solution in the fields of grid storage and electric vehicles.

AUTHOR INFORMATION

Corresponding Author
*steingart@princeton.edu.

Author Contributions
#Authors B.J.H. and A.H. equally contributed.

Notes
The authors declare no competing financial interest.

ACKNOWLEDGMENTS

REFERENCES

(1) Linden, D.; Reddy, T. B. *Handbook of Batteries*; McGraw Hill, 2002; vol *1e42*, p 4.

(2) Maskell, W. C.; Shaw, J.; Tye, F. L. Manganese Dioxide electrode—IV. Chemical and Electrochemical Reduction of an Electrolytic γ-MnO2. Reduction of- MnO_2. *Electrochim. Acta* **1981**, *26* (10), 1403−1410.

(3) Ohzuku, T.; Hirai, T. XRD and IR Studies on MnO_2/MnOOH systems. In *Proceedings of the Symposium on Manganese Dioxide Electrode Theory and Practice for Electrochemical Applications*; The Electrochemical Society, Inc., Pennington, NJ, 1985; vol 85−4, pp 141−157.

(4) Holton, D. M.; Maskell, W. C.; Tye, F. L. In *Power Sources 10*; Pearce, L., Ed.; The Paul Press: London, 1985.

(5) Boden, D.; Venuto, C. J.; Wisler, D.; Wylie, R. B. The Alkaline Manganese Dioxide Electrode: I. The Discharge Process. *J. Electrochem. Soc.* **1967**, *114* (5), 415−417.

(6) McBreen, J. The Electrochemistry of β-MnO_2 and γ-MnO_2 in Alkaline Electrolyte. *Electrochim. Acta* **1975**, *20* (3), 221−225.

(7) Mondoloni, C.; Laborde, M.; Rioux, J.; Andoni, E.; Lévy-Clément, C. Rechargeable Alkaline Manganese Dioxide Batteries: I. In Situ X-Ray Diffraction Investigation of the (EMD-Type) Insertion System. *J. Electrochem. Soc.* **1992**, *139* (4), 954−959.

(8) Van der Ven, A.; Morgan, D.; Meng, Y. S.; Ceder, G. Phase Stability of Nickel Hydroxides and Oxyhydroxides. *J. Electrochem. Soc.* **2006**, *153* (2), A210−A215.

(9) Ovsyannikov, S. V.; Abakumov, A. M.; Tsirlin, A. A.; Schnelle, W.; Egoavil, R.; Verbeeck, J.; Van Tendeloo, G.; Glazyrin, K. V.; Hanfland, M.; Dubrovinsky, L. Perovskite-like Mn2O3: A Path to New Manganites. *Angew. Chem.* **2013**, *125* (5), 1534−1538.

(10) Devaraj, S.; Munichandraiah, N. Effect of Crystallographic Structure of MnO_2 on Its Electrochemical Capacitance Properties. *J. Phys. Chem. C* **2008**, *112* (11), 4406−4417.

(11) Gallaway, J. W.; Menard, M.; Hertzberg, B.; Zhong, Z.; Croft, M.; Sviridov, L. A.; Turney, D. E.; Banerjee, S.; Steingart, D. A.; Erdonmez, C. K. Hetaerolite Profiles in Alkaline Batteries Measured by High Energy EDXRD. *J. Electrochem. Soc.* **2015**, *162* (1), A162−A168.

(12) Im, D.; Manthiram, A. Role of Bismuth and Factors Influencing the Formation of Mn_3O_4 in Rechargeable Alkaline Batteries Based on Bismuth-Containing Manganese Oxides. *J. Electrochem. Soc.* **2003**, *150* (1), A68−A73.

(13) Dzieciuch, M. A.; Gupta, N.; Wroblowa, H. S. Rechargeable Cells with Modified MnO_2 Cathodes. *J. Electrochem. Soc.* **1988**, *135* (10), 2415−2418.

(14) Bailey, M. R.; Donne, S. W. Structural Effects on the Cyclability of the Alkaline γ-MnO_2 Electrode. *Electrochim. Acta* **2011**, *56* (14), 5037−5045.

(15) Bezdička, P.; Grygar, T.; Klápště, B.; Vondrák, J. MnOx/C Composites as Electrode Materials. I. Synthesis, XRD and Cyclic Voltammetric Investigation. *Electrochim. Acta* **1999**, *45* (6), 913−920.

(16) Huang, X.; Yue, H.; Attia, A.; Yang, Y. Preparation and Properties of Manganese Oxide/Carbon Composites by Reduction of Potassium Permanganate with Acetylene Black. *J. Electrochem. Soc.* **2007**, *154* (1), A26−A33.

(17) Hertzberg, B.; Sviridov, L.; Stach, E. A.; Gupta, T.; Steingart, D. A Manganese-Doped Barium Carbonate Cathode for Alkaline Batteries. *J. Electrochem. Soc.* **2014**, *161* (6), A835−A840.

(18) Binder, L.; Jantscher, W.; Hofer, F.; Kothleitner, G. Production and Characterisation of Electrolytically Doped Manganese Dioxide. *J. Power Sources* **1998**, *70* (1), 1−7.

(19) Nartey, V. K.; Binder, L.; Huber, A. Production and Characterisation of Titanium Doped Electrolytic Manganese Dioxide for Use in Rechargeable Alkaline Zinc/manganese Dioxide Batteries. *J. Power Sources* **2000**, *87* (1−2), 205−211.

(20) Im, D.; Manthiram, A.; Coffey, B. Manganese(III) Chemistry in KOH Solutions in the Presence of Bi- or Ba-Containing Compounds and Its Implications on the Rechargeability of γ-MnO$_2$ in Alkaline Cells. *J. Electrochem. Soc.* **2003**, *150* (12), A1651−A1659.

(21) Li, X.; Li, Z.; Xia, T.; Dong, H.; Song, Y.; Wang, L. Rechargeability Improvement of δ-Type Chemical Manganese Dioxide with the Co-Doping of Bi and Ni in Alkaline Electrolyte. *J. Phys. Chem. Solids* **2012**, *73* (10), 1229−1234.

(22) Minakshi, M.; Singh, P.; Carter, M.; Prince, K. The Zn − MnO$_2$ Battery: The Influence of Aqueous LiOH and KOH Electrolytes on the Intercalation Mechanism. *Electrochem. Solid-State Lett.* **2008**, *11* (8), A145−A149.

(23) Minakshi, M.; Singh, P. Synergistic Effect of Additives on Electrochemical Properties of MnO$_2$ Cathode in Aqueous Rechargeable Batteries. *J. Solid State Electrochem.* **2012**, *16* (4), 1487−1492.

(24) Minakshi, M. Improved Performance of Bi2O3-Doped MnO2 Cathode on Rechargeability in LiOH Aqueous Cell. *J. Solid State Electrochem.* **2009**, *13* (8), 1209−1214.

(25) Minakshi, M. Alkaline-Earth Oxide Modified MnO$_2$ Cathode: Enhanced Performance in an Aqueous Rechargeable Battery. *Ind. Eng. Chem. Res.* **2011**, *50* (14), 8792−8795.

(26) Bard, A. J.; Faulkner, L. R. *Electrochemical Methods: Fundamentals and Applications*, 2nd ed.; Wiley, 2000.

(27) Croft, M.; Zakharchenko, I.; Zhong, Z.; Gurlak, Y.; Hastings, J.; Hu, J.; Holtz, R.; DaSilva, M.; Tsakalakos, T. Strain Field and Scattered Intensity Profiling with Energy Dispersive X-Ray Scattering. *J. Appl. Phys.* **2002**, *92* (1), 578−586.

(28) Rijssenbeek, J.; Gao, Y.; Zhong, Z.; Croft, M.; Jisrawi, N.; Ignatov, A.; Tsakalakos, T. In Situ X-Ray Diffraction of Prototype Sodium Metal Halide Cells: Time and Space Electrochemical Profiling. *J. Power Sources* **2011**, *196* (4), 2332−2339.

(29) Shen, Y.; Kordesch, K. The Mechanism of Capacity Fade of Rechargeable Alkaline Manganese Dioxide Zinc Cells. *J. Power Sources* **2000**, *87* (1−2), 162−166.

(30) Urfer, A.; Lawrance, G. A.; Swinkels, D. A. J. The Role of Particle Size in Cathode Optimization in Alkaline Primary Batteries. *J. Appl. Electrochem.* **2001**, *31* (3), 341−347.

(31) Nevers, D. R.; Peterson, S. W.; Robertson, L.; Chubbuck, C.; Flygare, J.; Cole, K.; Wheeler, D. R. The Effect of Carbon Additives on the Microstructure and Conductivity of Alkaline Battery Cathodes. *J. Electrochem. Soc.* **2014**, *161* (10), A1691−A1697.

(32) Wroblowa, H. S.; Gupta, N. Rechargeable Manganese Oxide Electrodes: Part II. Physically Modified Materials. *J. Electroanal. Chem. Interfacial Electrochem.* **1987**, *238* (1−2), 93−102.

(33) Abou-El-Sherbini, K. S.; Askar, M. H.; Schöllhorn, R. Hydrated Layered Manganese Dioxide:: III. Role of Bismuth Oxide on the Redox Behaviour of Hydrated Layered Manganese Dioxides. *Solid State Ionics* **2001**, *139* (1−2), 121−133.

(34) Bode, M.; Cachet, C.; Bach, S.; Pereira-Ramos, J.-P.; Ginoux, J. C.; Yu, L. T. Rechargeability of MnO2 in KOH Media Produced by Decomposition of Dissolved KMnO$_4$ and Bi (NO$_3$)$_3$ Mixtures I. Mn-Bi Complexes. *J. Electrochem. Soc.* **1997**, *144* (3), 792−801.

(35) Yu, L. T. Rechargeability of MnO$_2$ in KOH Media Produced by Decomposition of Dissolved KMnO$_4$ and Bi(NO$_3$)$_3$ Mixtures II. A Reaction Viewpoint on the Role of Bi. *J. Electrochem. Soc.* **1997**, *144* (3), 802−809.

(36) Qu, D. Y.; Conway, B. E.; Bai, L.; Zhou, Y. H.; Adams, W. A. Role of Dissolution of Mn(iii) Species in Discharge and Recharge of Chemically-Modified MnO$_2$ Battery Cathode Materials. *J. Appl. Electrochem.* **1993**, *23* (7), 693−706.

(37) Julien, C.; Massot, M.; Baddour-Hadjean, R.; Franger, S.; Bach, S.; Pereira-Ramos, J. P. Raman Spectra of Birnessite Manganese Dioxides. *Solid State Ionics* **2003**, *159* (3−4), 345−356.

(38) Li, N.; Patrissi, C. J.; Che, G.; Martin, C. R. Rate Capabilities of Nanostructured LiMnO$_4$ Electrodes in Aqueous Electrolyte. *J. Electrochem. Soc.* **2000**, *147* (6), 2044−2049.

(39) Paik, Y.; Bowden, W.; Richards, T.; Sirotina, R.; Grey, C. P. 2 H MAS NMR and SPECS Studies of γ-MnO2 Reduction in Zinc Alkaline Primary Batteries. *J. Electrochem. Soc.* **2004**, *151* (7), A998−A1011.